Journal of Magnetism and Magnetic Materials 432 (2017) 300–303

Contents lists available at ScienceDirect

Journal of Magnetism and Magnetic Materials

journal homepage: www.elsevier.com/locate/jmmm

Structural and magnetic properties evolution study method using a single ribbon-shaped sample

Javier A. Moya

Grupo Interdisciplinario en Materiales-IESIING, Universidad Católica de Salta, INTECIN UBA-CONICET, Salta, Argentina

ARTICLE INFO

Article history:
Received 21 December 2016
Received in revised form 30 January 2017
Accepted 3 February 2017
Available online 6 February 2017

ABSTRACT

A new type of study is presented for magnetic and structural characterization of amorphous or nanocrystalline metallic alloys in ribbon or wire-shaped samples. A single sample is subjecting to successive steps of flash isocurrent heat treatments with increasing duration in time, followed by a rapid cooling, while magneto-electric properties evolution are scanned in situ at room temperature. When one set of isocurrent heat treatments is finished, the annealing current is increased and a new set of isocurrent treatments starts. The properties studied were the saturation magnetization and the coercive field at 50 Hz, magnetic permeability at 100 kHz and electrical resistance from where we also obtained the crystalline fraction. The method was applied on two samples of Finemet-like alloys and the results were analyzed from the perspective of current literature. With the present method it is possible to obtain a general and meticulous understanding of the structural and magnetic evolution of the samples tested, with a considerable saving of time and samples.

1. Introduction

Heat treatments in metals can be performed in order to alter their properties either through structural relaxation (stress relief annealings) or phase-emerging annealings (crystallization or precipitation of second phases), both of which depend on the kinetics of the atoms. Usually, the heat treatments are performed by subjecting the material into an environment with the desired annealing temperature. One type of non-conventional heat treatment is the Joule heating technique which employs the electrical resistance of the material (an electrically conductive material) to produce the necessary heat by injecting a high density electrical current enough for activating the transformations.

Amorphous metal ribbons are obtained by rapidly quenching the alloy from the liquid state, with a cooling rate of about 10^6 K/s, employing melt spinning or planar flow casting techniques. Their main use today is as soft magnetic materials in high efficiency transformers cores, current sensors, magnetic shielding, etc. These materials are especially attractive to be subjected to different annealing treatments because of their residual stresses accumulated during the production process and their metastable structure condition which can evolve towards more stable ones (like the nanocrystalline structure). Moreover, the ribbon-shaped of the material – with thickness of 20 or 40 μm – and the relative high resistivity value make these materials particularly suitable to be Joule heated as no high power currents are necessary to produce the annealings and a relative uniform distribution of the temperature is reached.

Early works in current annealing on amorphous ribbons began in 1983 [1] with applying currents up to 5 A at times up to 20 s, in order to stress relaxed the material and improve its magnetic properties. From then on, many works have been made on this type of alloys with different aims, such as the study of the technique itself (e.g., [2–4]), the growth of nanocrystals [5,6], the improvement of the material properties [7,8], the study of phase transitions [9], etc.

In a previous paper [10], we introduce the Joule heating scanning structure system (JHS3, see Fig. 1), a device with the ability to perform successive isochronal rectangular pulses of increasing (or decreasing) annealing current on amorphous ribbons while measuring magnetic and electric resistance properties in situ at room and at high temperature. The rapid quenching produced on the sample once the electrical pulse is finished freezes the high temperature structure ([11,12]) and in this instance the different properties are measured at room temperature. Then, with the rapid heating produced by the successive pulse, the structure would continue its structural evolution from the condition where it was frozen in the previous pulse and, during this period of time, the properties are measured at high temperature. In Fig. 2 a heating pulse of 5 s duration and 1 A intensity is shown together with the evolution of the electrical resistance on a nanocrystalline Finemet™ alloy ribbon producing a full crystallized structure, i.e.,

E-mail address: jmoya.fi.uba@gmail.com

http://dx.doi.org/10.1016/j.jmmm.2017.02.005
0304-8853/

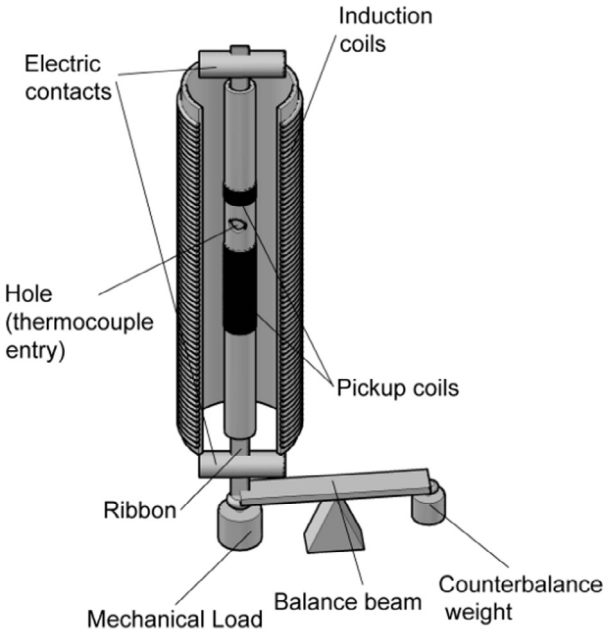

Fig. 1. Coils and ribbon sample set up employed for the study [10].

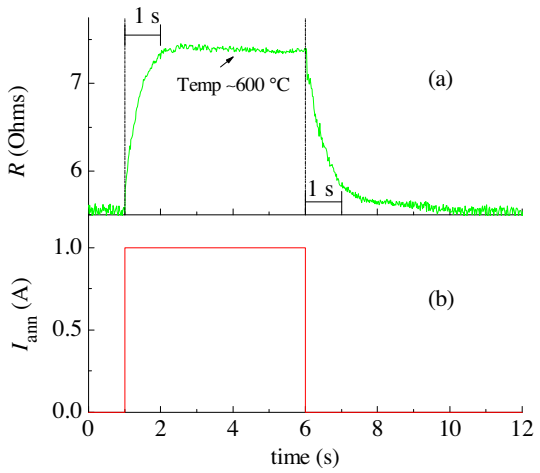

Fig. 2. Time evolution of the resistance in a nanocrystalline ribbon (a) with the current annealing pulse (b).

reaching temperature $\geqslant$600 °C. Then, the heating and cooling rates are both estimated in $\geqslant$600 °C/s. This high cooling rate value is achieved mainly by the low thermal inertia of the ribbon or wire-shaped samples, and can be increased with some external cooling system. In this paper, we present the results obtained with the JHS3 in a novel isocurrent time depending heat treatments which consist in a series of successive rectangular pulses of annealing current with increasing duration in time.

2. Experimental

For the set-up of this technique, amorphous samples of Finemet-like alloys were chosen because they were extensively studied in the past and the results can be easily compared with those obtained in the present study. Two 12 cm long, 0.7 mm wide and ~20 μm thick amorphous ribbons samples of chemical composition $Fe_{73.5}Si_{22.5-x}B_xNb_3Cu_1$ with $x = 6$ and 12 (samples B6 and B12, respectively) were submitted into the JHS3 device and performed 50 successive steps of annealing treatments. These consist in injecting a constant annealing current (isocurrent), e.g., I_{ann} = 350 mA, during 50 increasing periods of time, t_i, starting at t_1 = 0.1 s, and finishing at t_{50} = 5 s. The time increment between each successive period was kept constant at Δt = 0.1 s. Every time one of the 50 periods of time ended, the annealing current was set to I_{ann} = 0 mA during some seconds until the entire system returned to room temperature according to the thermocouple measurement (15 s on average). At this instance, the saturation magnetization, M_s, the coercive field, H_c (both under a maximum alternating applied field of H = 1.5 kA/m at 50 Hz), the initial permeability, μ_r (H_{rms} = 0.4 A/m at 100 kHz) and the room temperature electrical resistance, R_{rt}, were measured in the JHS3 device at room temperature while the electrical resistance at high temperature, R_{temp}, was also obtained during the current annealing. On the same sample, we repeated N series (N = 10 and 14 for B6 and B12 samples, respectively) of the same procedure of 50 steps heat treatments for a constant annealing current increased in ΔI_{ann} = 50 mA with respect to the previous isocurrent annealing (e.g., I_{ann} = 350, 400, 450, 500, 550, 600, 650, 700, 750 and 800 mA for N = 10 series). This combination of time-dependent isocurrent heat treatments with the N series is schematized on Fig. 3 where we represent the I_{ann} vs. t_i. Only the N series for I_{ann} = 350, 400 and 800 mA are plotted with five steps each (i.e., t_1 to t_4 and t_{50}). The breaks in the abscissa correspond to where the room temperature properties were measured.

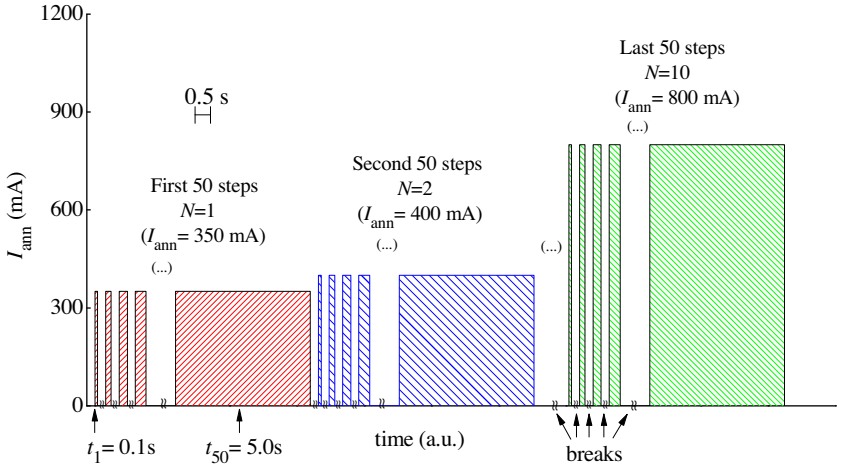

Fig. 3. Schema of some successive steps of annealing current applied to sample B6.

3. Results and discussion

Fig. 4 shows the results of the evolution of the measured properties with the heat treatments for both samples. All the series, N, of heat treatments were plotted together for convenience of representation. Time unit in abscissa is referred to the corresponding series of heat treatments in the way $T = (N - 1)\cdot 5\ \mathrm{s} + t_i$. For example, $T = 17.3$ s, corresponds to the 4th series of heat treatment ($N = 4$, $I_{ann} = 500$ mA) with $t_i = 2.3$ s. Due to differences in chemical composition of the alloys and in section of the samples, the initial electrical resistances of both samples were different (14.9 and 17.4 Ω for B6 and B12, respectively) and therefore, the I_{ann} necessary to produce the structural changes is different for each sample. We adjusted the abscissa of the graphs of the two sample alloys so that structural changes match (approximately) in both alloys for a better understanding of the experimental results. In Fig. 4 (a) and (e) are plotted together the evolution of both, the R_{rt} and R_{temp}, with the annealing time for the alloys B12 and B6 respectively. The magnetic properties M_s, H_c and μ_r determined at room temperature are plotted in Fig. 4(b) and (f), (c) and (g), and (d) and (h), for alloys B12 and B6, respectively.

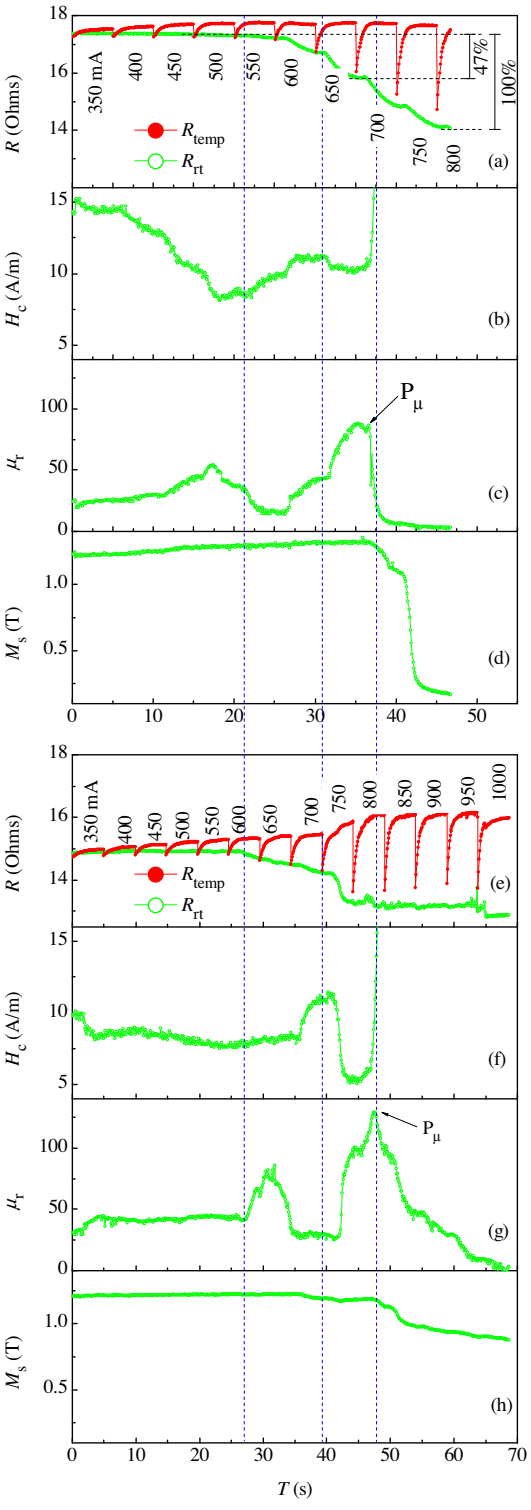

Fig. 4. Evolution of the measured properties with heat treatments for samples B12 in (a) to (d) and B6 in (e) to (h).

The behaviors of the measured properties clearly show the three evolution steps present in these alloys: I) structural relaxation, II) nanocrystallization and III) grain grow and boride crystallization. During the first step, the structural relaxation releases the mechanical strains produced by the rapid quenching during the sample production. This is clearly observed in the decrease of H_c and the increase of μ_r values, as the soft magnetic properties are governed principally by the magnetoelastic anisotropy ($K_{el} = \sigma\cdot\lambda_s$, where σ is the mechanical stress and λ_s the saturation magnetostriction constant) in the amorphous stage. The fact that greater changes in H_c are observed in the B12 sample may be due to a higher value of internal stresses related to a smaller thickness (or higher quenching rates) of the sample compared with the B6 one. Indeed, once sample B12 has relaxed (at $T \sim 20$ s), its H_c reaches a similar value to that of sample B6 (i.e., $H_c \sim 8$ A/m). M_s and R_{rt} present no or minors changes.

Step II initiates with Cu clustering process producing pinning wall centers and increasing the mechanical stresses; as a consequence, magnetic hardening is observed before the nanocrystallisation process. Subsequently, the nanocrystallisation process produces several effects on magnetic anisotropies and saturation magnetization of the alloys, depending almost exclusively on the nanograins size and composition, and on its crystalline fraction. The fact that B12 alloy is magnetically softener than the B6 one would be due to the higher Si content in nanocrystals resulting in a lower magnetostriction and magnetocrystalline anisotropies (i.e., a better magnetostriction balance between amorphous and crystalline phases, and a neglected value of the average magnetocrystalline anisotropy, respectively) [13]. The Si content in the amorphous precursor determines the chemical composition of the crystalline phase in the nanocrystalline state. In the B12 nanocrystalline alloy (with Si content of 10.5% in amorphous precursor) the Si content in crystalline phase is ~17%, while for the B6 one (with 16.5% Si in amorphous precursor) it is ~21% Si [14]. This is also consistent with the behavior of M_s with nanocrystallization process on both samples [14]. The total saturation magnetization will depend on a certain balance between the fractions of nanocrystalline and amorphous remnant phases present in the material. Nanocrystals in sample B12 have a higher M_s than the ones in sample B6 (due to the higher Fe content in the former) and consequently, the total M_s increases with nanocrystallisation process, contrary to the behavior of M_s in the B6 sample. During the scanning in the second stage, a small sharp peak in the permeability was observed in both samples (marked with Pμ in Fig. 4 (c) and (g), less pronounced in B12 alloy), just before entering the third stage. This peak, also observed in other studies (e.g., see the graphical abstract, where the results obtained in the B6 alloy with an $\Delta I_{ann} = 100$ mA is shown), coincides with the beginning of the H_c deterioration, just after the minimum reached during the nanocrystallisation process. The origin of this peak is not clear

for us, but it could be related to the occurrence of a local bias field produced by the precipitation of some small hard magnetic particles but confirmation of this would require further studies.

Finally, on stage III, the longer annealing times and/or the higher annealing temperatures induce the coarsening of the α-Fe (Si) nanograins and the precipitation of boride phases that deteriorate the soft magnetic properties. As it can be seen in Fig. 4, sample B12 deteriorates faster than sample B6 as a consequence of the higher B content that promotes the formation of more boron compounds [14].

Complementary, we can also make an estimation of the crystallization fraction from the electrical resistance measurements [15]. Considering a linear dependence of the total room temperature resistance, R_T, with crystalline fraction, v_{cr}, we have that $R_T = R_{cr} \cdot v_{cr} + R_{am}(1 - v_{cr})$, where R_{am} and R_{cr} are the resistance of the amorphous and fully crystallized states, respectively. This results in a rough estimation of a $v_{cr} = 47$ and 76% for B12 and B6 alloys, respectively, showing the same tendency as in [14] (i.e., ∼60 and ∼79%, respectively) evaluated from thermomagnetic investigations. An example of this calculus is shown in Fig. 4(a).

4. Conclusions

Performing some series of time-increasing isocurrent heat treatments with increasing annealing currents on each series, a comprehensive and meticulous scanning of the magnetic and structural properties was performed over two nanocrystalline ribbon-shaped alloys. Apart from the individual measured properties, this amount of data allowed us to make further analysis on the magneto-structural behavior of the two nanocrystalline alloys by comparing the results obtained on only one sample of each alloy (e.g., crystalline fraction, iron content in nanocrystals and boride formation ability). The method described here reduces significant time in samples preparation while it shows in great detail the structural changes occurred. This type of studies can improve the current way of carrying out these kinds of structural and magnetic studies and can be adapted for the determination of other properties in non-magnetic alloys.

Acknowledgments

This work was supported by PICT-2014-2324 project of the MINCyT, Argentina.

References

[1] T. Jagielinski, Flash annealing of amorphous alloys, IEEE Trans. Magn. 19 (1983) 1925–1927, http://dx.doi.org/10.1109/TMAG.1983.1062629.
[2] P. Allia, M. Baricco, M. Knobel, P. Tiberto, F. Vinai, An exact model of d.c. joule heating in amorphous metallic ribbons, Mater. Sci. Eng. A 179–180 (1994) 361–365, http://dx.doi.org/10.1016/0921-5093(94)90227-5.
[3] N. Zabala, J.M. Barandiaran, Temperature study in flash annealing of metallic glasses, J. Phys. Appl. Phys. 28 (1995) 2607–2611, http://dx.doi.org/10.1088/0022-3727/28/12/032.
[4] P. Allia, P. Tiberto, M. Baricco, F. Vinai, Dc Joule heating of amorphous metallic ribbons: experimental aspects and model, Rev. Sci. Instrum. 64 (1993) 1053, http://dx.doi.org/10.1063/1.1144177.
[5] P. Allia, P. Tiberto, M. Baricco, M. Knobel, F. Vinai, Nanostructured materials for soft magnetic applications produced by fast dc Joule heating, IEEE Trans. Magn. 30 (1994) 4797–4799, http://dx.doi.org/10.1109/20.334225.
[6] J.A. Moya, V. Cremaschi, F.C.S. Silva, M. Knobel, H. Sirkin, Influence of the heat treatment method on magnetic and mechanical properties of the $Fe_{73.5}Si_{13.5}B9Nb_3Cu_1$ alloy, J. Magn. Magn. Mater. 226–230 (2001) 1522–1523, http://dx.doi.org/10.1016/S0304-8853(00)00945-8.
[7] P. Allia, P. Tiberto, M. Baricco, F. Vinai, Improved ductility of nanocrystalline $Fe_{73.5}Nb_3Cu_1Si_{13.5}B_9$ obtained by direct-current joule heating, Appl. Phys. Lett. 63 (1993) 2759, http://dx.doi.org/10.1063/1.110326.
[8] I.V. Okulov, I.V. Soldatov, M.F. Sarmanova, I. Kaban, T. Gemming, K. Edström, J. Eckert, Flash Joule heating for ductilization of metallic glasses, Nat. Commun. 6 (2015) 7932, http://dx.doi.org/10.1038/ncomms8932.
[9] P. Rougier, R. Krishnan, Stability studies in Fe–Ni based amorphous ribbons: some refinement, IEEE Trans. Magn. 23 (1987) 2134–2135, http://dx.doi.org/10.1109/TMAG.1987.1065626.
[10] J.A. Moya, Joule heating scanning structure system, Rev. Sci. Instrum. 87 (2016) 085116, http://dx.doi.org/10.1063/1.4961472.
[11] N.S. Mitrovic, S.R. Djukic, S.B. Djuric, Crystallization of the Fe–Cu–M–Si–B (M = Nb, V) amorphous alloys by direct-current Joule heating, IEEE Trans. Magn. 36 (2000) 3858–3862, http://dx.doi.org/10.1109/20.908401.
[12] F.C.S. da Silva, E.F. Ferrari, M. Knobel, Precipitation and dissolution of Co granules in CuCo alloys: reverse effects of Joule heating, J. Appl. Phys. 86 (1999) 7170, http://dx.doi.org/10.1063/1.371808.
[13] J.A. Moya, Improving soft magnetic properties in FINEMET-like alloys. A study, J. Alloys Compd. 622 (2015) 635–639, http://dx.doi.org/10.1016/j.jallcom.2014.10.124.
[14] G. Herzer, Nanocrystalline soft magnetic alloys, in: K.H.J. Buschow (Ed.), Handb. Magn. Mater., Elsevier, Amsterdam, 1997, p. 415.
[15] P. Allia, M. Baricco, P. Tiberto, F. Vinai, Kinetics of the amorphous-to-nanocrystalline transformation in $Fe_{73.5}Cu_1Nb_3Si_{13.5}B_9$, J. Appl. Phys. 74 (1993) 3137, http://dx.doi.org/10.1063/1.354581.